JACS
JOURNAL OF THE AMERICAN CHEMICAL SOCIETY
pubs.acs.org/JACS
Communication

Supramolecular Assembly of Fused Macrocycle-Cage Molecules for Fast Lithium-Ion Transport

Yuzhe Wang, Kaiyang Wang, Qing Ai, Stephen D. Funni, Ashutosh Garudapalli, Qiyi Fang, Suin Choi, Gangbin Yan, Shayan Louie, Chong Liu, Jun Lou, Judy J. Cha, Jingjie Yeo, Zexin Jin,* and Yu Zhong*

Cite This: https://doi.org/10.1021/jacs.4c08558
Read Online
ACCESS | Metrics & More | Article Recommendations | Supporting Information

ABSTRACT: We report a new supramolecular porous crystal assembled from fused macrocycle-cage molecules. The molecule comprises a prismatic cage with three macrocycles radially attached. The molecules form a nanoporous crystal with one-dimensional (1D) nanochannels. The supramolecular porous crystal can take up lithium-ion electrolytes and achieve an ionic conductivity of up to 8.3×10^{-4} S/cm. Structural analysis and density functional theory calculations reveal that efficient Li-ion electrolyte uptake, the presence of 1D nanochannels, and weak interactions between lithium ions and the crystal enable fast lithium-ion transport. Our findings demonstrate the potential of fused macrocycle-cage molecules as a new design motif for ion-conducting molecular crystals.

This paper describes a supramolecular porous crystal (SPC) assembled from new fused macrocycle-cage building blocks, which exhibits ultrahigh lithium-ion conductivity. SPCs provide a fertile material platform for sensing,[1−4] ion transport,[5−7] gas adsorption,[8−10] and molecular separation,[11−14] owing to their well-defined pores and chemical versatility. Among these applications, ion-conducting SPCs hold great potential for energy storage applications.[15−18] One approach to creating ion-conducting SPCs is to use intrinsically porous molecules such as macrocycles and molecular cages.[19−21] For example, Dichtel et al. reported an organic nanotube assembled by macrocycles that exhibits a lithium-ion conductivity of 3.92×10^{-5} S/cm.[22] Alternatively, multiarmed monomers that can provide directional interactions can be used to form three-dimensional SPCs.[23,24] For instance, Xie and co-workers utilized racemic 9,9′-diphenyl-[2,2′-bifluorene]-9,9′-diol (DPFOH) enantiomers to construct porous crystals, achieving a Li-ion conductivity of 1.8×10^{-4} S/cm.[18]

The exploration of new designs for SPCs is highly desired to achieve Li-ion conductivity beyond the current benchmarks. Generally, there are three principles guiding the design of ion-conducting SPCs. First, multiarmed molecules with high symmetry are preferred as they tend to assemble into porous structures in the crystal. Second, these molecules should form crystals through strong intermolecular interactions like hydrogen bonding,[6,25] $\pi-\pi$ interaction,[26,27] and shape complementarity.[19] Additionally, the interactions between molecules and Li ions should be weak to facilitate the free movement of Li ions in nanopores.[7]

Here, we report an SPC assembled from novel topological molecules containing a fused macrocycle and molecular cage structure. Figure 1 displays the design of the fused macrocycle-cage (**MC**) molecule. **MC** features a prismatic cage at the center with three macrocycles radially attached, creating a unique three-dimensional propeller-like structure. This molecular architecture enables the **MC**s to self-assemble into nanoporous single crystals via shape complementarity and hydrogen bonds, forming one-dimensional (1D) nanochannels

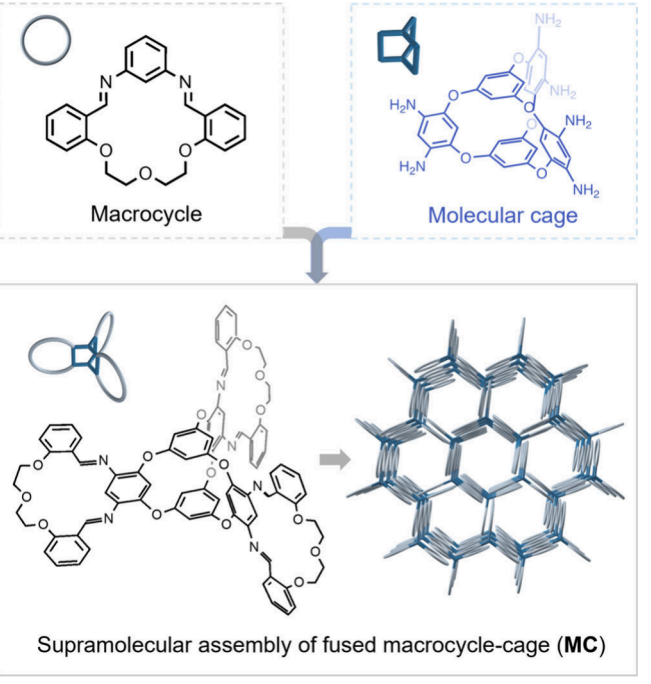

Figure 1. Structural design of supramolecular porous crystal from fused macrocycle-cage (**MC**).

Received: June 24, 2024
Revised: August 20, 2024
Accepted: September 5, 2024

Scheme 1. Synthesis of MC

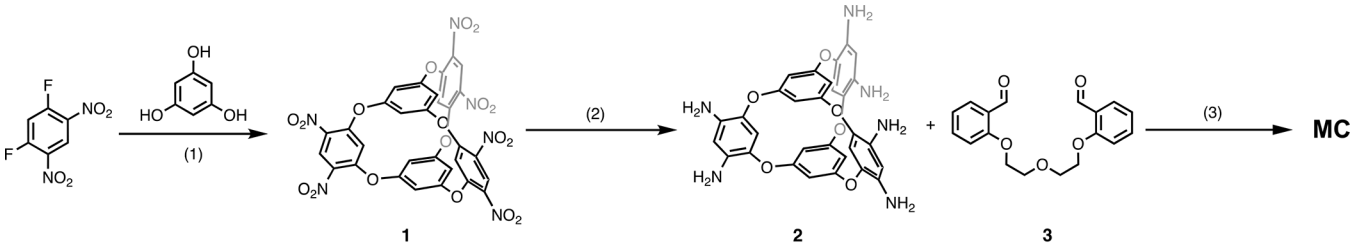

Key: (1) K_2CO_3, DMSO, rt, 24h (83%); (2) $SnCl_2$, conc. HCl, 24h (81%); (3) CH_3COOH, Dioxane, 80°C, 24h, (69%)

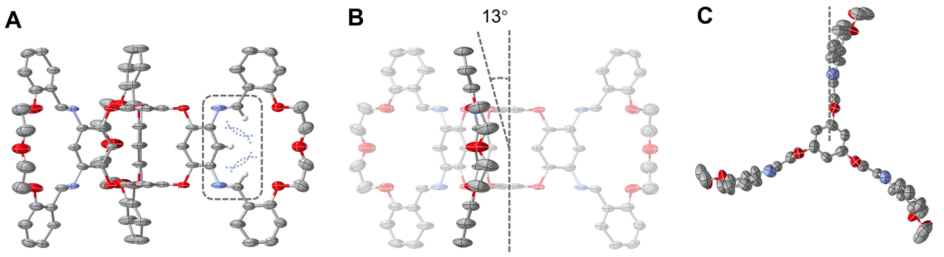

Figure 2. (A) Side view of **MC** obtained from the single-crystal X-ray structure. The probability for the ellipsoid model is 25%. The dashed-line box highlights steric hindrance from hydrogen atoms within the macrocycle. Carbon = gray, nitrogen = blue, oxygen = red, hydrogen = white. Hydrogen atoms are omitted for clarity except for the ones in the box. (B) Side view of **MC** and bend angle of the macrocycle with respect to the axial direction. (C) Top view of **MC**. The dashed line indicates the radial direction.

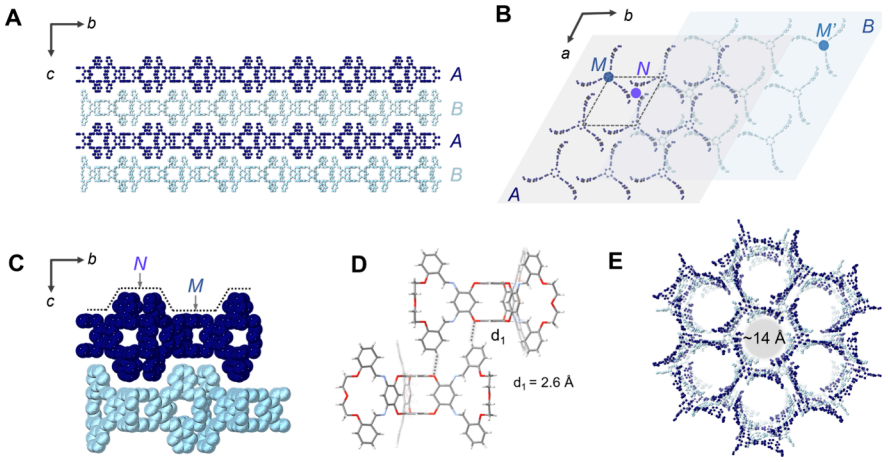

Figure 3. (A) Side view of the **MC** crystal structure. Layer *A* and layer *B* are marked by different colors, respectively. (B) The interlayer stacking mode of **MC**. (C) Side view of the **MC** crystal showing the alternating convex and concave surfaces in each layer and the interlayer shape complementarity. (D) Two **MC** molecules in adjacent layers interact with each other via hydrogen bonds. The hydrogen bonds are indicated by dashed lines. (E) Top view of the **MC** crystal structure.

suitable for ion transport. Furthermore, **MC** crystals can incorporate lithium salt during the crystal growth process, resulting in a highly ionically conductive nanoporous material. The Li-ion conductivity in the single crystal is measured to be 8.3×10^{-4} S/cm, which is among the highest values for SPCs.[7,18,22,28−31] Experimental results and DFT calculations suggest that efficient Li-ion uptake, the presence of 1D ion channels, and weak interactions between molecules and Li ions could facilitate Li ions' hopping transport. Our results suggest a new pathway for the design of ion-conducting SPCs.

Scheme 1 shows the synthesis of **MC**. A hexa-amine-substituted molecular cage (**2**) was first synthesized according to previously reported methods.[32,33] The cage molecule then reacts with 3 equiv of 1,7-bis(2′-formylphenyl)-1,4,7-trioxaheptane (**3**) via imine condensation, resulting in **MC** as a yellow solid in 69% yield. The structure of **MC** was confirmed by nuclear magnetic resonance (NMR), Fourier transform infrared (FTIR), and high-resolution mass spectroscopy (HRMS). The Supporting Information contains the details for the syntheses and characterizations of **MC** and its precursors (Figures S1−S6).

Single crystals of **MC** were obtained by slow diffusion of methanol vapor into the chloroform solution of **MC**. The resulting crystals are either hexagonal rods or hexagonal plates (Figure S7). From the single crystal structure, we identified the molecular conformation of **MC**, as shown in Figure 2. Due to the steric hindrance of the three hydrogen atoms within the macrocycles (Figure 2A), the peripheral macrocycles are curved away from planarity. When viewed from the side, the top and bottom parts of the macrocycle are bent toward the

https://doi.org/10.1021/jacs.4c08558
J. Am. Chem. Soc. XXXX, XXX, XXX−XXX

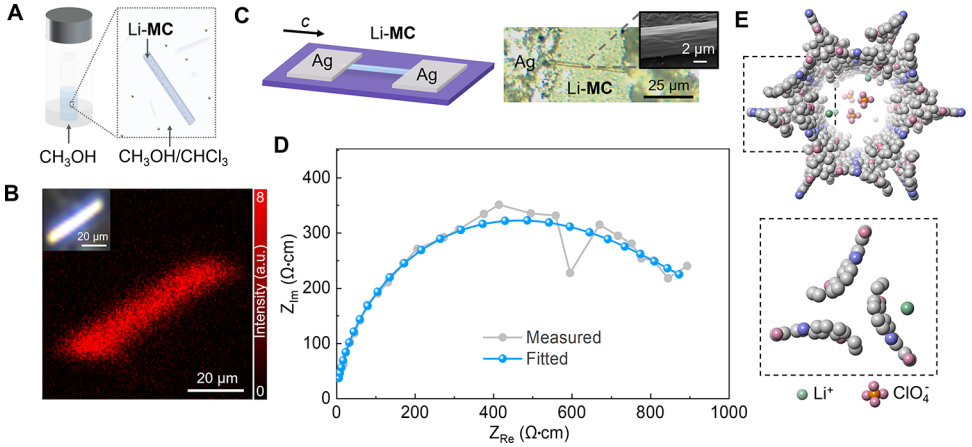

Figure 4. (A) Schematic of the growth of Li-**MC** single crystals. (B) ToF-SIMS image of the Li^+ distribution in a Li-**MC** crystal. Inset: optical image of the corresponding Li-**MC** crystal. The image shows the average intensity of Li^+ corresponding to sputtering time from 100 to 500 s. (C) Schematic (left) and optical image (right) of a two-terminal electronic device made from a Li-**MC** crystal. Inset: SEM image of the Li-**MC** crystal. (D) Nyquist plots of the AC impedance data obtained from the device in (C). (E) Top: schematic of Li-ion transport in the 1D channel. Bottom: DFT optimized geometry showing the optimal binding site for Li ions in the Li-**MC** crystal.

same side, forming an approximately 13° angle with respect to the axial direction (Figure 2B). When viewed from the top, the three macrocycles are twisted away from the radial direction (Figure 2C). We note that the three macrocycles are always curved in the same direction, either clockwise or all anticlockwise. The propeller structure and contorted macrocycles lead to a unique packing of **MC**s in crystals (vide infra).

MC molecules self-assemble into an SPC with 1D nanochannels. Figure 3 displays the structure of the **MC** crystals. The **MC** crystals have a hexagonal lattice (see the details of the crystal structure in Table S1). The molecules form layered structures in the *a*−*b* plane (Figures 3A and S8). The unit cell comprises two layers of molecules, denoted as layers *A* and *B*, respectively. The **MC** molecules are organized into hexagonal structures, with the centers of **MC**s occupying the vertices (i.e., *M* point in layer *A* and *M*′ point in layer *B* in Figure 3B). Within each layer, the macrocycles from three adjacent **MC**s are aligned against each other, forming an angstrom-scale triangle. The center of this triangle is denoted as the *N* point in layer *A* (Figure 3B). Along the *c*-axis, the molecular monolayers stack layer by layer in an alternating "*A*−*B*" mode. In each layer, the peripheral macrocycles in the **MC** molecules curve in the same direction. In layer *A*, the macrocycles swing clockwise, while, in layer *B*, they swing counterclockwise (Figure 3B). The centers of the triangle (e.g., *N* in layer *A*) formed by the macrocycles sit on top of the centers of **MC**s in the next layer (e.g., *M*′ in layer *B*), resulting in an *A*−*B* stacking pattern (Figure 3B).

The single crystal structure reveals that the presence of *A*−*B* stacking arises from two types of interactions. First, the stacking is driven by the interlayer shape complementarity (Figure 3C). In each layer, the supramolecular assembly of **MC**s forms alternating concave and convex surfaces (Figure 3C and Figure S9). The center of the convex surface is at point *N*, while the center of the concave surface is at point *M*. The concave surfaces in layer *A* perfectly match the convex surfaces in layer *B*, and vice versa. Second, the **MC** molecules in adjacent layers are bound by strong hydrogen bonds. The H···O distance in the C−H···O hydrogen bonds (d_1 in Figure 3D) is 2.6 Å. Together, the shape complementarity and the interlayer hydrogen bonds lead to the *A*−*B* stacking of **MC**s in the crystal. As a result, the supramolecular assembly of **MC** molecules forms 1D nanochannels with a diameter of about 14 Å along the *c*-axis (Figure 3E).

The 1D nanochannels make **MC** crystals an ideal material for ion transport. To prepare ion-containing supramolecular solids, we grew crystals from an **MC** solution in a mixed methanol/chloroform solvent with the addition of lithium perchlorate (Figure 4A). We found that this method yielded microplate and microrod crystals similar to those obtained from the pure **MC** solution (Figure S10). We term these crystals Li-**MC**. Although we were not able to resolve the single crystal structure of Li-**MC**, powder X-ray diffraction (PXRD) patterns reveal that Li-**MC** and **MC** crystals share the same structure (Figure S11). The varied intensity in the diffraction peaks is likely due to the uptake of lithium salt in the crystal. It is known that nanopores in crystals can be filled with solvent molecules and ions from the mother liquor during the crystallization process. Given that the Li-**MC** crystals retain the same crystal structure as the pure **MC** crystals, we envision that 1D nanochannels in the Li-**MC** crystals might be filled with a $LiClO_4$ electrolyte solution. To verify the presence of Li ions in the crystals, we used time-of-flight secondary ion mass spectrometry (ToF-SIMS) to analyze the element distributions in the bulk crystals. The ToF-SIMS images clearly show a uniform Li distribution in the bulk Li-**MC** crystal (Figure 4B and Figure S12). Energy dispersive X-ray spectroscopy (EDS) mapping also confirms the enhanced intensity of Cl in the Li-**MC** crystal compared to that in the **MC** crystal, which may arise from the existence of perchlorate counterions in the Li-**MC** crystals (Figures S13 and S14). Both ToF-SIMS and EDS measurements suggest that the Li-**MC** crystal has efficient lithium-ion electrolyte uptake. Thus, the Li-**MC** crystals may serve as a supramolecular lithium-ion electrolyte and exhibit ionic conduction through the 1D channels.

To measure the ionic conductivity of the Li-**MC** crystals, we fabricated a two-terminal device on a Li-**MC** microrod by depositing silver electrodes on the two ends of the crystal (Figure 4C). The microrod crystal was used so that the 1D nanochannels (along the *c*-axis) aligned with the desired ion transport direction across the two electrodes. Electrochemical impedance spectroscopy (EIS) measurements show that the

https://doi.org/10.1021/jacs.4c08558
J. Am. Chem. Soc. XXXX, XXX, XXX−XXX

Li-**MC** crystal exhibits remarkable ionic conductivity up to 8.3 × 10^{-4} S/cm (Figure 4D and Figure S15). To the best of our knowledge, this value is among the highest reported for molecular nanoporous crystals (Table S2).[7,18,22,28−31] As a comparison, the **MC** crystals without Li ions do not exhibit any detectable conductivity, showing insulating characteristics. Notably, our ion-conductivity measurements were conducted on an organic single crystal, as opposed to using polycrystalline powders. This measurement represents the intrinsic ionic transport property of the Li-**MC** supramolecular porous crystals.

To understand ionic transport within the Li-**MC** crystals, we investigated the status and concentration of the lithium and perchlorate ions. Raman spectroscopy reveals that the perchlorate anions exist as free solvated ions within the Li-**MC** crystals (Figure S16). This suggests that the Li-**MC** crystals take up both ions and solvent molecules from the electrolyte. Inductively coupled plasma mass spectrometry (ICP-MS) revealed a Li-ion concentration of approximately 0.02 wt % in the crystals, corresponding to a molar concentration of 0.04 M within the 1D nanochannels. This concentration is comparable to the initial concentration (0.01 M) of $LiClO_4$ in the solution, indicating efficient uptake of the $LiClO_4$ electrolyte. The presence of solvated ions within the Li-**MC** crystals also implies weak interactions between the Li ions and the **MC** molecules. To gain insight into the interactions between Li ions and **MC** crystals, we performed density functional theory (DFT) calculations on a system that contains Li ions and a fraction of the 1D nanochannel walls. Our results suggest that the preferred site for Li ions is in the proximity of a macrocyclic unit of **MC** molecules (Figure 4E and Figure S17). However, the interaction between the Li ions and the **MC** molecule is moderate, with a calculated free energy of ∼0.2 eV. This value is smaller than the solvation energy between Li ion and methanol/chloroform.[34] The similarity in PXRD patterns between Li-**MC** and **MC** powders also suggests that there are weak interactions between Li ions and **MC**s. The reduced binding energy between Li ions and **MC** may facilitate the transport of solvated Li ions in the nanochannel.[7,34] Therefore, we hypothesize that the efficient uptake of $LiClO_4$ electrolyte, 1D nanochannels, and weak interactions between Li ions and **MC** molecules collectively contribute to the high ionic conductivity of the Li-**MC** crystals.[35]

In summary, the fused macrocycle-cage molecule represents a new design motif for ion-conducting SPCs. Leveraging self-assembly, the creation of 1D nanochannels in Li-**MC** crystals offers an efficient pathway for Li ion transport. Moreover, the supramolecular assembly of **MC** crystals in an electrolyte solution proves a facile method to make ion-conducting solid-state electrolytes. This concept can be applied to design versatile fused macrocycle-cage molecules with tunable properties and enhanced ion transport performance. Our work potentially opens new avenues to the design of SPC-based solid-state electrolytes for safe lithium-ion batteries.

■ ASSOCIATED CONTENT

Supporting Information

The Supporting Information is available free of charge at https://pubs.acs.org/doi/10.1021/jacs.4c08558.

Synthetic details and characterization, X-ray crystallography, crystal images, element mapping, additional experiment procedures, and calculation details (PDF)

Accession Codes

CCDC 2278971 contains the supplementary crystallographic data for this paper. These data can be obtained free of charge via www.ccdc.cam.ac.uk/data_request/cif, or by emailing data_request@ccdc.cam.ac.uk, or by contacting The Cambridge Crystallographic Data Centre, 12 Union Road, Cambridge CB2 1EZ, UK; fax: +44 1223 336033.

■ AUTHOR INFORMATION

Corresponding Authors

Zexin Jin − *Department of Chemistry, Columbia University, New York, New York 10027, United States; Research Center for Industries of the Future, Westlake University, Hangzhou, Zhejiang 310030, China; School of Engineering, Westlake University, Hangzhou, Zhejiang 310030, China;* orcid.org/0000-0002-4971-3656; Email: jinzexin@westlake.edu.cn

Yu Zhong − *Department of Materials Science and Engineering, Cornell University, Ithaca, New York 14853, United States;* orcid.org/0000-0001-8631-2213; Email: yz2833@cornell.edu

Authors

Yuzhe Wang − *Department of Materials Science and Engineering, Cornell University, Ithaca, New York 14853, United States;* orcid.org/0009-0004-8186-6435

Kaiyang Wang − *Department of Materials Science and Engineering, Cornell University, Ithaca, New York 14853, United States;* orcid.org/0000-0002-1529-0958

Qing Ai − *Department of Materials Science and NanoEngineering, Rice University, Houston, Texas 77005, United States;* orcid.org/0000-0002-6086-5431

Stephen D. Funni − *Department of Materials Science and Engineering, Cornell University, Ithaca, New York 14853, United States*

Ashutosh Garudapalli − *Department of Materials Science and Engineering, Cornell University, Ithaca, New York 14853, United States*

Qiyi Fang − *Department of Materials Science and Engineering, Cornell University, Ithaca, New York 14853, United States*

Suin Choi − *Pritzker School of Molecular Engineering, University of Chicago, Chicago, Illinois 60637, United States*

Gangbin Yan − *Pritzker School of Molecular Engineering, University of Chicago, Chicago, Illinois 60637, United States;* orcid.org/0000-0002-4711-9063

Shayan Louie − *Department of Chemistry, Columbia University, New York, New York 10027, United States*

Chong Liu − *Pritzker School of Molecular Engineering, University of Chicago, Chicago, Illinois 60637, United States;* orcid.org/0000-0003-4851-7888

Jun Lou − *Department of Materials Science and NanoEngineering, Rice University, Houston, Texas 77005, United States;* orcid.org/0000-0002-4351-9561

Judy J. Cha − *Department of Materials Science and Engineering, Cornell University, Ithaca, New York 14853, United States*

Jingjie Yeo − *Sibley School of Mechanical and Aerospace Engineering, Cornell University, Ithaca, New York 14853, United States;* orcid.org/0000-0002-6462-7422

https://doi.org/10.1021/jacs.4c08558
J. Am. Chem. Soc. XXXX, XXX, XXX−XXX

Complete contact information is available at:
https://pubs.acs.org/10.1021/jacs.4c08558

Funding

Y.W. was supported by the engineering learning initiatives (ELI) undergraduate research award under the Dean Archer Undergraduate Research Program.

Notes

The authors declare no competing financial interest.

■ ACKNOWLEDGMENTS

This work was supported by Cornell University through startup funding. Yuzhe Wang was supported by the engineering learning initiatives (ELI) undergraduate research award under the Dean Archer Undergraduate Research Program. The authors acknowledge the use of facilities and instrumentation supported by NSF through the Cornell University Materials Research Science and Engineering Center DMR-1719875, the Columbia University Materials Research Science and Engineering Center DMR-2011738, and the Columbia University MRI award CHE-1531632. STEM and EDS characterizations were supported by DOE BES DE-SC0023905. Research reported in this publication was supported by the Office of The Director of the National Institutes of Health under Award Number S10OD026749. The content is solely the responsibility of the authors and does not necessarily represent the official views of the National Institutes of Health. J.L. acknowledges funding from The Welch Foundation Grant C-1716. Z.J. acknowledges funding from Research Center for Industries of the Future at Westlake University and Westlake Education Foundation. We thank Qiuming Yu for helping with EIS measurements.

■ ABBREVIATIONS

MC, macrocycle-cage molecule; ^{1}H NMR, proton nuclear magnetic resonance; PXRD, powder X-ray diffraction; FT-IR, Fourier-transform infrared spectroscopy; EDS, energy dispersive X-ray spectroscopy; HRMS, high-resolution mass spectroscopy; EIS, electrochemical impedance spectroscopy; ICP-MS, inductively coupled plasma mass spectrometry; DFT, density functional theory; ToF-SIMS, time-of-flight secondary ion mass spectrometry

■ REFERENCES

(1) Wang, B.; He, R.; Xie, L.-H.; Lin, Z.-J.; Zhang, X.; Wang, J.; Huang, H.; Zhang, Z.; Schanze, K. S.; Zhang, J.; Xiang, S.; Chen, B. Microporous Hydrogen-Bonded Organic Framework for Highly Efficient Turn-up Fluorescent Sensing of Aniline. *J. Am. Chem. Soc.* **2020**, *142* (28), 12478−12485.

(2) Liu, Y.; Shen, J.; Sun, C.; Ren, C.; Zeng, H. Intramolecularly Hydrogen-Bonded Aromatic Pentamers as Modularly Tunable Macrocyclic Receptors for Selective Recognition of Metal Ions. *J. Am. Chem. Soc.* **2015**, *137* (37), 12055−12063.

(3) Tang, X.; Jiang, H.; Si, Y.; Rampal, N.; Gong, W.; Cheng, C.; Kang, X.; Fairen-Jimenez, D.; Cui, Y.; Liu, Y. Endohedral Functionalization of Chiral Metal-Organic Cages for Encapsulating Achiral Dyes to Induce Circularly Polarized Luminescence. *Chem.* **2021**, *7* (10), 2771−2786.

(4) Wang, Y.; Han, N.; Ma, C.-Q.; Liu, H.; Yu, S.; Wang, R.; Thakur, V. K.; Xing, L.-B. A Novel Strategy of Constructing 2D Supramolecular Organic Framework Sensor for the Identification of Toxic Metal Ions. *Nano Materials Science* **2023**, *5* (3), 335−342.

(5) Yoon, M.; Suh, K.; Kim, H.; Kim, Y.; Selvapalam, N.; Kim, K. High and Highly Anisotropic Proton Conductivity in Organic Molecular Porous Materials. *Angew. Chem., Int. Ed. Engl.* **2011**, *50* (34), 7870−7873.

(6) Yang, Z.; Zhang, N.; Lei, L.; Yu, C.; Ding, J.; Li, P.; Chen, J.; Li, M.; Ling, S.; Zhuang, X.; Zhang, S. Supramolecular Proton Conductors Self-Assembled by Organic Cages. *JACS Au* **2022**, *2* (4), 819−826.

(7) Park, J. H.; Suh, K.; Rohman, M. R.; Hwang, W.; Yoon, M.; Kim, K. Solid Lithium Electrolytes Based on an Organic Molecular Porous Solid. *Chem. Commun. (Camb.)* **2015**, *51* (45), 9313−9316.

(8) Yang, W.; Greenaway, A.; Lin, X.; Matsuda, R.; Blake, A. J.; Wilson, C.; Lewis, W.; Hubberstey, P.; Kitagawa, S.; Champness, N. R.; Schröder, M. Exceptional Thermal Stability in a Supramolecular Organic Framework: Porosity and Gas Storage. *J. Am. Chem. Soc.* **2010**, *132* (41), 14457−14469.

(9) Doonan, C. J.; Tranchemontagne, D. J.; Glover, T. G.; Hunt, J. R.; Yaghi, O. M. Exceptional Ammonia Uptake by a Covalent Organic Framework. *Nat. Chem.* **2010**, *2* (3), 235−238.

(10) Xie, Y.; Pan, T.; Lei, Q.; Chen, C.; Dong, X.; Yuan, Y.; Maksoud, W. A.; Zhao, L.; Cavallo, L.; Pinnau, I.; Han, Y. Efficient and Simultaneous Capture of Iodine and Methyl Iodide Achieved by a Covalent Organic Framework. *Nat. Commun.* **2022**, *13* (1), 2878.

(11) Yin, Q.; Pang, K.; Feng, Y.-N.; Han, L.; Morsali, A.; Li, X.-Y.; Liu, T.-F. Hydrogen-Bonded Organic Frameworks in Solution Enables Continuous and High-Crystalline Membranes. *Nat. Commun.* **2024**, *15* (1), 634.

(12) Wu, Y.; Zhou, J.; Li, E.; Wang, M.; Jie, K.; Zhu, H.; Huang, F. Selective Separation of Methylfuran and Dimethylfuran by Nonporous Adaptive Crystals of Pillararenes. *J. Am. Chem. Soc.* **2020**, *142* (46), 19722−19730.

(13) He, A.; Jiang, Z.; Wu, Y.; Hussain, H.; Rawle, J.; Briggs, M. E.; Little, M. A.; Livingston, A. G.; Cooper, A. I. A Smart and Responsive Crystalline Porous Organic Cage Membrane with Switchable Pore Apertures for Graded Molecular Sieving. *Nat. Mater.* **2022**, *21* (4), 463−470.

(14) He, Y.; Xiang, S.; Chen, B. A Microporous Hydrogen-Bonded Organic Framework for Highly Selective C2H2/C2H4 Separation at Ambient Temperature. *J. Am. Chem. Soc.* **2011**, *133* (37), 14570−14573.

(15) Cao, Y.; Wang, M.; Wang, H.; Han, C.; Pan, F.; Sun, J. Covalent Organic Framework for Rechargeable Batteries: Mechanisms and Properties of Ionic Conduction. *Adv. Energy Mater.* **2022**, *12* (20), 2200057.

(16) Tang, X.; Pang, J.; Dong, J.; Liu, Y.; Bu, X.-H.; Cui, Y. Supramolecular Assembly Frameworks(SAFs): Shaping the Future of Functional Materials. *Angew. Chem., Int. Ed. Engl.* **2024**, *136*, No. e202406956.

(17) Jeong, K.; Park, S.; Jung, G. Y.; Kim, S. H.; Lee, Y.-H.; Kwak, S. K.; Lee, S.-Y. Solvent-Free, Single Lithium-Ion Conducting Covalent Organic Frameworks. *J. Am. Chem. Soc.* **2019**, *141* (14), 5880−5885.

(18) Wang, S.-S.; Liu, Y.-R.; Yu, X.; Zhou, Y.; Zhong, T.-T.; Li, Y.-T.; Xie, L.-H.; Huang, W. Supramolecular Non-Helical One-Dimensional Channels and Microtubes Assembled from Enantiomers of Difluorenol. *Angew. Chem., Int. Ed. Engl.* **2021**, *60* (8), 3979−3983.

(19) Tozawa, T.; Jones, J. T. A.; Swamy, S. I.; Jiang, S.; Adams, D. J.; Shakespeare, S.; Clowes, R.; Bradshaw, D.; Hasell, T.; Chong, S. Y.; Tang, C.; Thompson, S.; Parker, J.; Trewin, A.; Bacsa, J.; Slawin, A. M. Z.; Steiner, A.; Cooper, A. I. Porous Organic Cages. *Nat. Mater.* **2009**, *8* (12), 973−978.

(20) Zhu, H.; Chen, L.; Sun, B.; Wang, M.; Li, H.; Stoddart, J. F.; Huang, F. Applications of Macrocycle-Based Solid-State Host-Guest Chemistry. *Nat. Rev. Chem.* **2023**, *7* (11), 768−782.

(21) Zhu, Q.; Qu, H.; Avci, G.; Hafizi, R.; Zhao, C.; Day, G. M.; Jelfs, K. E.; Little, M. A.; Cooper, A. I. Computationally Guided Synthesis of a Hierarchical [4[2 + 3]+6] Porous Organic 'Cage of Cages.'. *Nat. Synth.* **2024**, *3*, 825−834.

(22) Strauss, M. J.; Hwang, I.; Evans, A. M.; Natraj, A.; Aguilar-Enriquez, X.; Castano, I.; Roesner, E. K.; Choi, J. W.; Dichtel, W. R. Lithium-Conducting Self-Assembled Organic Nanotubes. *J. Am. Chem. Soc.* **2021**, *143* (42), 17655−17665.

(23) Maly, K. E.; Gagnon, E.; Maris, T.; Wuest, J. D. Engineering Hydrogen-Bonded Molecular Crystals Built from Derivatives of Hexaphenylbenzene and Related Compounds. *J. Am. Chem. Soc.* **2007**, *129* (14), 4306−4322.
(24) Huang, Q.; Li, W.; Mao, Z.; Qu, L.; Li, Y.; Zhang, H.; Yu, T.; Yang, Z.; Zhao, J.; Zhang, Y.; Aldred, M. P.; Chi, Z. An Exceptionally Flexible Hydrogen-Bonded Organic Framework with Large-Scale Void Regulation and Adaptive Guest Accommodation Abilities. *Nat. Commun.* **2019**, *10* (1), 3074.
(25) Han, B.; Wang, H.; Wang, C.; Wu, H.; Zhou, W.; Chen, B.; Jiang, J. Postsynthetic Metalation of a Robust Hydrogen-Bonded Organic Framework for Heterogeneous Catalysis. *J. Am. Chem. Soc.* **2019**, *141* (22), 8737−8740.
(26) Karki, S.; Karas, L. J.; Wang, X.; Wu, J. I.; Miljanić, O. Š. Synthesis and Columnar Organization of Partially Fluorinated Dehydrobenz[18]Annulenes. *Cryst. Growth Des.* **2022**, *22* (4), 2076−2081.
(27) Mastalerz, M.; Schneider, M. W.; Oppel, I. M.; Presly, O. A Salicylbisimine Cage Compound with High Surface Area and Selective CO2/CH4 Adsorption. *Angew. Chem., Int. Ed. Engl.* **2011**, *50* (5), 1046−1051.
(28) Nakamura, T.; Akutagawa, T.; Honda, K.; Underhill, A. E.; Coomber, A. T.; Friend, R. H. A Molecular Metal with Ion-Conducting Channels. *Nature* **1998**, *394* (6689), 159−162.
(29) Moriya, M.; Kitaguchi, H.; Nishibori, E.; Sawa, H.; Sakamoto, W.; Yogo, T. Molecular Ionics in Supramolecular Assemblies with Channel Structures Containing Lithium Ions. *Chemistry* **2012**, *18* (48), 15305−15309.
(30) Li, J.; Qi, J.; Jin, F.; Zhang, F.; Zheng, L.; Tang, L.; Huang, R.; Xu, J.; Chen, H.; Liu, M.; Qiu, Y.; Cooper, A. I.; Shen, Y.; Chen, L. Room Temperature All-Solid-State Lithium Batteries Based on a Soluble Organic Cage Ionic Conductor. *Nat. Commun.* **2022**, *13* (1), 1−11.
(31) Tanaka, K.; Tago, Y.; Kondo, M.; Watanabe, Y.; Nishio, K.; Hitosugi, T.; Moriya, M. High Li-Ion Conductivity in $LiN(SO_2F)_2(NCCH_2CH_2CN)_2$ Molecular Crystal. *Nano Lett.* **2020**, *20* (11), 8200−8204.
(32) Zhu, Q.; Wang, X.; Clowes, R.; Cui, P.; Chen, L.; Little, M. A.; Cooper, A. I. 3D Cage COFs: A Dynamic Three-Dimensional Covalent Organic Framework with High-Connectivity Organic Cage Nodes. *J. Am. Chem. Soc.* **2020**, *142* (39), 16842−16848.
(33) Ji, C.; Su, K.; Wang, W.; Chang, J.; El-Sayed, E.-S. M.; Zhang, L.; Yuan, D. Tunable Cage-Based Three-Dimensional Covalent Organic Frameworks. *CCS Chem.* **2022**, *4* (9), 3095−3105.
(34) Pliego, J. R., Jr; Miguel, E. L. M. Absolute Single-Ion Solvation Free Energy Scale in Methanol Determined by the Lithium Cluster-Continuum Approach. *J. Phys. Chem. B* **2013**, *117* (17), 5129−5135.
(35) Wiers, B. M.; Foo, M.-L.; Balsara, N. P.; Long, J. R. A Solid Lithium Electrolyte via Addition of Lithium Isopropoxide to a Metal-Organic Framework with Open Metal Sites. *J. Am. Chem. Soc.* **2011**, *133* (37), 14522−14525.

https://doi.org/10.1021/jacs.4c08558
J. Am. Chem. Soc. XXXX, XXX, XXX−XXX